Light-enabled reversible self-assembly and tunable optical properties of stable hairy nanoparticles

Yihuang Chen[a,b], Zewei Wang[a], Yanjie He[a], Young Jun Yoon[a], Jaehan Jung[a], Guangzhao Zhang[b,1], and Zhiqun Lin[a,1]

[a]School of Materials Science and Engineering, Georgia Institute of Technology, Atlanta, GA 30332; and [b]Faculty of Materials Science and Engineering, South China University of Technology, 510640 Guangzhou, China

The ability to dynamically organize functional nanoparticles (NPs) via the use of environmental triggers (temperature, pH, light, or solvent polarity) opens up important perspectives for rapid and convenient construction of a rich variety of complex assemblies and materials with new structures and functionalities. Here, we report an unconventional strategy for crafting stable hairy NPs with light-enabled reversible and reliable self-assembly and tunable optical properties. Central to our strategy is to judiciously design amphiphilic star-like diblock copolymers comprising inner hydrophilic blocks and outer hydrophobic photoresponsive blocks as nanoreactors to direct the synthesis of monodisperse plasmonic NPs intimately and permanently capped with photoresponsive polymers. The size and shape of hairy NPs can be precisely tailored by modulating the length of inner hydrophilic block of star-like diblock copolymers. The perpetual anchoring of photoresponsive polymers on the NP surface renders the attractive feature of self-assembly and disassembly of NPs on demand using light of different wavelengths, as revealed by tunable surface plasmon resonance absorption of NPs and the reversible transformation of NPs between their dispersed and aggregated states. The dye encapsulation/release studies manifested that such photoresponsive NPs may be exploited as smart guest molecule nanocarriers. By extension, the star-like block copolymer strategy enables the crafting of a family of stable stimuli-responsive NPs (e.g., temperature- or pH-sensitive polymer-capped magnetic, ferroelectric, upconversion, or semiconducting NPs) and their assemblies for fundamental research in self-assembly and crystallization kinetics of NPs as well as potential applications in optics, optoelectronics, magnetic technologies, sensory materials and devices, catalysis, nanotechnology, and biotechnology.

nanoreactor | stable hairy nanoparticles | photoresponsive polymers | reversible self-assembly | tunable optical properties

The use of external triggers to regulate self-assembly of nanoparticles (NPs) (1) represents an important step toward the creation of an exciting variety of functional structures and materials from nanoscopic building blocks for applications in water treatment (2), biochemical detector (3), colorimetric sensing (4), and controlled delivery (5). Among various types of triggers such as temperature (6), pH (7), and solvent polarity (8) used to direct self-assembly of NPs, light has emerged as a distinct and highly effective stimulus as it carries several unique and advantageous attributes (9, 10). Light can be easily and rapidly employed and removed (9). Furthermore, light is capable of being delivered remotely and instantaneously to the targeted locations in a non-invasive manner. More importantly, light of varied intensities and wavelengths can be readily tuned to enable the precise control over the assembly and disassembly of NPs with engineered structures and properties (9) for use in catalytic system (10), self-erasable paper (11), and temperature nanosensor (12).

To impart the repeated self-assembly and disassembly of NPs by employing light, a crucial prerequisite is to either graft chromophore-containing ligands [small molecules (10–17) or polymers (18, 19)] onto the NP surface (i.e., forming photoresponsive NPs) or place nonphotoresponsive NPs in the

chromophore-containing medium (11, 20). Clearly, two approaches noted above require proper passivation of NP with a layer of ligands to disperse them in solution. However, due to the inherent nature of NPs, functional end groups in ligands that bind to NP need to be highly selective [e.g., polar groups such as –SH, –OH, and –NH_2 for metal NPs, and polar charged groups such as –PO_3^{2-}, –SO_3^-, and –COO^-/COOH for metal oxide NPs (16)] to yield strongly ligated NPs. As a result, tedious synthetic procedures are generally invoked to obtain ligands with desirable terminal functional groups (10, 11). More importantly, despite the efforts noted above, the binding between ligand and NP is usually still relatively weak. Ligand dissociation may occur over a long period of time and is likely aggravated upon the change in experimental conditions, thereby leading to reduced surface coverage of ligands and eventually agglomeration of NPs (21). For example, although gold–thiol (Au–SH) interaction is widely recognized as a semicovalent bond, it is destroyed by oxidation or thermal desorption (16) when Au NPs passivated with photoresponsive SH-terminated ligands are irradiated with UV light, resulting in the loss of photoresponsive capability and the NP aggregation (22). Obviously, it remains challenging to create truly stable photoresponsive NPs.

Herein, we developed a robust strategy for crafting stable hairy photoresponsive plasmonic Au NPs that afford light-enabled reversible self-assembly and thus tailorable optical properties of NPs. These hairy Au NPs can be reversibly and reliably self-assembled and disassembled upon irradiation with 365- and 254-nm UV lights, respectively, as corroborated by tunable surface plasmon resonance (SPR) absorption of Au NPs and their reversible dispersion-to-aggregation-to-dispersion transition. The key to our strategy is to capitalize on rationally designed amphiphilic star-like poly(acrylic acid)-*block*-poly(7-methylacryloyloxy-4-methylcoumarin) (denoted

Significance

This work reports a versatile and robust strategy for creating monodisperse plasmonic nanoparticles (NPs) intimately and permanently capped with photoresponsive polymers via capitalizing on amphiphilic star-like diblock copolymer nanoreactors. The reversibly assembled nanostructures comprising photoresponsive NPs may exhibit a broad range of new attributes, functions, and applications as a direct consequence of size-dependent physical property from individual NP and the collective property originated from the NP interaction due to their close proximity within nanostructure.

PAA-*b*-PMAMC) diblock copolymers as nanoreactors to create in situ photoresponsive Au NPs. Star-like PAA-*b*-PMAMC is synthesized by sequential atom transfer radical polymerization (ATRP) of *tert*-butyl acrylate (*t*BA) and 7-methylacryloyloxy-4-methylcoumarin (MAMC) using a β-cyclodextrin (β-CD)-based macroinitiator [i.e., yielding star-like poly(*tert*-butyl acrylate)-*block*-poly(7-methylacryloyloxy-4-methylcoumarin) (P*t*BA-*b*-PMAMC)], followed by hydrolysis of inner hydrophobic P*t*BA into hydrophilic PAA. Star-like PAA-*b*-PMAMC diblock copolymers form structurally stable spherical unimolecular micelles in the mixed solvents of the proper ratio. The strong coordination interaction between the metal moieties of Au precursors and the inner hydrophilic PAA blocks occurs within spherical micelles that preferentially concentrate the precursors (23, 24), leading to the nucleation and growth of PMAMC-capped Au NPs (i.e., hairy Au NPs). Such photoresponsive NPs can be exploited as smart guest molecule nanocarriers. In conjunction with tunable optical properties, this class of NPs presents attractive potentials for use in catalysis, surface-enhanced Raman spectroscopy, nanodetector, biology, etc.

The hallmarks of our star-like block copolymer nanoreactor strategy are fivefold. First, as ATRP is a living free-radical polymerization technique, it affords superior controllability over the molecular weight (MW) of polymer. Therefore, it enables the synthesis of star-like diblock copolymers with tunable MWs and low polydispersity index (PDI) of PAA and PMAMC blocks, thus leading to the accurate control over the size of Au NPs and the length of outer photoresponsive PMAMC blocks. Second, it renders the efficient synthesis of monodisperse spherical NPs as star-like block copolymers form stable unimolecular micelles in which the inner and outer blocks are covalently connected to effectively maintain the spherical shape of micelles under various experimental conditions. This contrasts sharply to the use of conventional micelles formed via self-assembly of amphiphilic linear block copolymers as template for NP synthesis, where the size and shape of conventional micelles depend sensitively on concentration, solvent properties, pH, temperature, etc. Thus, a slight variation of these experimental conditions likely results in NPs with nonuniform size and shape. Third, compared with Au NPs capped with small ligands through interacting with func-

tional –SH end group as noted above (16), the intimately and permanently tethered PMAMC blocks enabled by the preexisting strong covalent bonding between PAA and PMAMC chains in star-like PAA-*b*-PMAMC nanoreactors can effectively suppress the potential damage of Au-PMAMC linkage when subjected to UV irradiation, thereby imparting robust, reliable, and reversible light-enabled self-assembly and disassembly of Au NPs. Fourth, in sharp contrast to small-molecule coumarin-containing ligands or polymer ligands having only one coumarin unit at the chain end, each repeat unit in the PMAMC block possesses one coumarin moiety. Such high population of coumarin affords a fast and efficient light-triggered reversible self-assembly of PMAMC-capped Au NPs with tunable optical properties. Fifth, conceptually, as appropriate precursors that are amenable to the star-shaped unimolecular nanoreactor strategy are quite diverse, a large array of monodisperse polymer-capped NPs with desired functionality and design complexity can be conveniently created.

Results

Synthesis of Unimolecular Star-Like P*t*BA-*b*-PMAMC Diblock Copolymers.
Fig. 1 depicts the synthetic route to PMAMC-capped Au NPs by capitalizing on amphiphilic unimolecular star-like PAA-*b*-PMAMC diblock copolymers as nanoreactors (*Materials and Methods*). First, 21 hydroxyl groups on β-CD were thoroughly esterified to yield 21-Br-β-CD (25–28) (Fig. 1, *Upper Center*). Subsequently, sequential ATRP of *t*BA and MAMC (Fig. 1, *Center Right*) monomers by employing the 21-Br-β-CD as macroinitiator yielded a family of unimolecular star-like P*t*BA-*b*-PMAMC diblock copolymers. Because of living free-radical polymerization characteristic, ATRP entailed the synthesis of star-like P*t*BA (Fig. 1, *Upper Right*) and P*t*BA-*b*-PMAMC (Fig. 1, *Lower* fourth panel) with well-controlled MW and low PDI of each block. The inner hydrophobic P*t*BA blocks were hydrolyzed into hydrophilic PAA blocks using trifluoroacetic acid (TFA), producing amphiphilic star-like PAA-*b*-PMAMC (Fig. 1, *Lower* third panel). The proton NMR (^{1}H NMR) measurements corroborated the successful synthesis of MAMC monomer (*SI Appendix*, Fig. S1) and star-like P*t*BA (*SI Appendix*, Fig. S2), P*t*BA-*b*-PMAMC (*SI Appendix*, Fig. S3). During the hydrolysis by TFA to yield star-like PAA-*b*-PMAMC, no

Fig. 1. Synthetic strategy. PMAMC-capped Au nanoparticles with tunable size were prepared in situ by capitalizing on amphiphilic star-like PAA-*b*-PMAMC diblock copolymers as nanoreactors.

undesired reaction (e.g., hydrolysis of lactone in PMAMC) was found (*SI Appendix*, Figs. S4–S6). It is notable that, compared with the conventional micelle prepared via self-assembly of linear amphiphilic block copolymers, each amphiphilic PAA-*b*-PMAMC arm in star-like copolymer nanoreactor is covalently linked to the β-CD–based macroinitiator core, forming a structurally stable spherical unimolecular micelle (25–27, 29, 30).

In Situ Crafting of Au NPs Permanently Capped with Photoresponsive Polymer Chains. Uniform plasmonic Au NPs capped with PMAMC chains that are originally covalently connected to the inner PAA chains were crafted in situ by utilizing amphiphilic star-like PAA-*b*-PMAMC diblock copolymers as nanoreactors (i.e., forming PMAMC-capped plasmonic Au NPs that can be regarded as hairy Au NPs; Fig. 1, *Lower* first panel). The star-like PAA-*b*-PMAMC nanoreactors were first dissolved in the *N,N*-dimethylformamide (DMF)/benzyl alcohol (BA) mixed solvents (DMF/BA of 7/3 by volume), followed by the addition of precursors HAuCl$_4$·3H$_2$O. As DMF is a good solvent for both PAA and PMAMC blocks while BA is a good solvent for PAA block only, star-like PAA-*b*-PMAMC diblock copolymers form stable unimolecular micelles with compact spherical shape composed of the expanded coil-like inner PAA chains and the collapsed outer PMAMC chains. This facilitated the preferential partition of HAuCl$_4$·3H$_2$O within the inner PAA compartment of spherical unimolecular micelle (Fig. 1, *Lower* second panel). The strong coordination interaction between the metal moieties of HAuCl$_4$·3H$_2$O and the carboxyl groups (−COOH) of PAA (23, 24, 31) led to the nucleation and growth of Au NPs intimately tethered with photoresponsive PMAMC chains.

Notably, the MWs (i.e., lengths) of PAA and PMAMC blocks with narrow PDI can be precisely tailored by controlling the ATRP time of each block during the nanoreactor synthesis due to the living characteristic of ATRP (32), which in turn yielded monodisperse size-tunable Au NPs and length-varied PMAMC block, respectively. *SI Appendix*, Table S2 summarizes the structural parameters of each block in a series of synthesized star-like diblock copolymers and the corresponding diameters of Au NPs. The hydrodynamic diameter, D_h, of star-like PAA homopolymers in DMF was measured by dynamic light scattering (DLS) (*SI Appendix*, Fig. S7).

Quite intriguingly, the selection of proper DMF/BA volume ratio as the mixed solvents exerted a crucial influence in producing monodisperse PMAMC-capped Au NPs (*SI Appendix*, Fig. S8). When pure DMF is employed, star-like PAA-*b*-PMAMC (i.e., sample A in *SI Appendix*, Table S2) can be simply dissolved with fully expanded chain conformation from the β-CD–based macroinitiator core as DMF is a good solvent for both PAA and PMAMC blocks. As BA is a good solvent for PAA while a nonsolvent for PMAMC, the addition of BA causes the outer PMAMC blocks to collapse while the inner PAA blocks still retain the coil-like conformation, which in turn imparts a good encapsulation of inorganic precursors. When the DMF/BA volume ratios were 9/1 (*SI Appendix*, Fig. S8*A*) and 5/5 (*SI Appendix*, Fig. S8*C*), the resulting Au NPs had relatively irregular size and shape. However, at the 7/3 DMF/BA volume ratio, Au NPs with the best uniformity were achieved (*SI Appendix*, Fig. S8*B*). This observation can be rationalized by considering the solubility of each block in the mixed solvents of different volume ratios (*SI Appendix*, Scheme S1). At high volume ratio of DMF/BA (i.e., 9/1), star-like PAA-*b*-PMAMC diblock copolymer displays a spherical macromolecular structure with outer slightly contracted PMAMC chains (*SI Appendix*, Scheme S1, *Upper Left*). Such loosely collapsed PMAMC chains are incapable of confining the precursors within the PAA compartment, thus yielding relatively irregular Au NPs (*SI Appendix*, Fig. S8*A* and Scheme S1, *Upper Right*). With an increased DMF/

BA volume ratio to 7/3, well-defined structurally stable micelles comprising more compact outer PMAMC chains and inner expanded PAA chains were yielded (*SI Appendix*, Scheme S1, *Center Left*), facilitating the maximum loading of precursors to form uniform Au NPs (*SI Appendix*, Fig. S8*B* and Scheme S1, *Center Right*). As more BA was added (at DMF/BA of 5/5 by volume), the outer PMAMC chains significantly collapsed due to unfavorable interaction between BA and the PMAMC chains. This effectively hindered the incorporation of precursors into the inner PAA regime (*SI Appendix*, Scheme S1, *Lower Left*), resulting in the formation of smaller NPs with decreased uniformity (*SI Appendix*, Fig. S8*C* and Scheme S1, *Lower Right*).

It is interesting to note that the rational design on the length of outer PMAMC chains in star-like PAA-*b*-PMAMC diblock copolymer played a key role in crafting high-quality Au NPs of uniform size and good dispersibility (Fig. 2 *A–C*). As noted above, the MW of PMAMC chains can be readily tuned by varying the reaction time during the ATRP of MAMC monomers. In addition to star-like PAA-*b*-PMAMC diblock copolymers with a 13,800 MW of outer PMAMC block used above (sample A in *SI Appendix*, Table S2, and Fig. 2*B*), two other star-like PAA-*b*-PMAMC diblock copolymers were prepared from the same star-like P*t*BA (hydrolyzed into PAA) with relatively low (i.e., 2,700 per PMAMC; short length) and high (i.e., 35,100 per PMAMC; long length) MWs of PMAMC chains, respectively. They were also employed as nanoreactors for synthesis of Au NPs. It is not surprising that neither of these two nanoreactors led to the formation of monodisperse Au NPs using the same 7/3 DMF/BA mixed solvents (sample B in *SI Appendix*, Table S2, Fig. 2*A*, and sample C in *SI Appendix*, Table S2, Fig. 2*C*), which can be understood as follows. In the 7/3 DMF/BA mixed solvents, the outer PMAMC chains in both cases also collapse due to unfavorable interaction between PMAMC and BA, as discussed above (*SI Appendix*, Scheme S1). When the PMAMC chain is short (2,700 per arm), the collapsed short PMAMC chains cannot effectively cover the entire surface of the PAA regime loaded with Au precursors (Fig. 2*D*, *Upper Left*), yielding heavily aggregated irregular Au NPs (Fig. 2*A*; Fig. 2*D*, *Upper Right*). Conversely, for the long PMAMC chains (35,100 per arm), the outer collapsed PMAMC chains are so densely covered that Au precursors can hardly enter the PAA compartment (Fig. 2*D*, *Lower Left*). As a result, instead of NPs, only cluster-like Au nanocrystals formed within nanoreactors without obvious aggregation (Fig. 2 *C* and *D*, *Lower Right*). We note that the effects of the volume ratio of the mixed solvents and the PMAMC MW discussed above were further substantiated by a suite of detailed characterizations on star-like PAA-*b*-PMAMC (*SI Appendix*, Table S2, samples A–C) at various DMF/BA volume ratios, including the size measurements (*SI Appendix*, Fig. S9), the evaluation of the permeability of PMAMC chains (*SI Appendix*, Fig. S10 and Scheme S2), and their use as nanoreactors for in situ Au NP formation (*SI Appendix*, Figs. S11 and S12). On the basis of the observation discussed above, smaller-sized monodisperse PMAMC-capped Au NPs with a diameter of 9.8 ± 0.5 nm were also readily crafted using sample E (*SI Appendix*, Fig. S13 and Table S2). Unless otherwise specified, PMAMC-capped Au NPs employed for all characterizations including light-enabled reversible self-assembly described below are those with a diameter of 14.9 ± 0.3 nm crafted using sample A in *SI Appendix*, Table S2.

A representative X-ray diffraction (XRD) pattern of PMAMC-capped Au NPs is shown in *SI Appendix*, Fig. S14. The peaks at scattering angle 2θ of 38.21°, 44.72°, 64.74°, 77.53°, and 81.32° correspond to the diffraction from the (111), (200), (220), (311), and (222) crystal planes of fcc Au, respectively, which is in good agreement with the standard XRD profile of bulk Au. The slightly broadened peaks are due to the nanosized Au NPs. Obviously, the
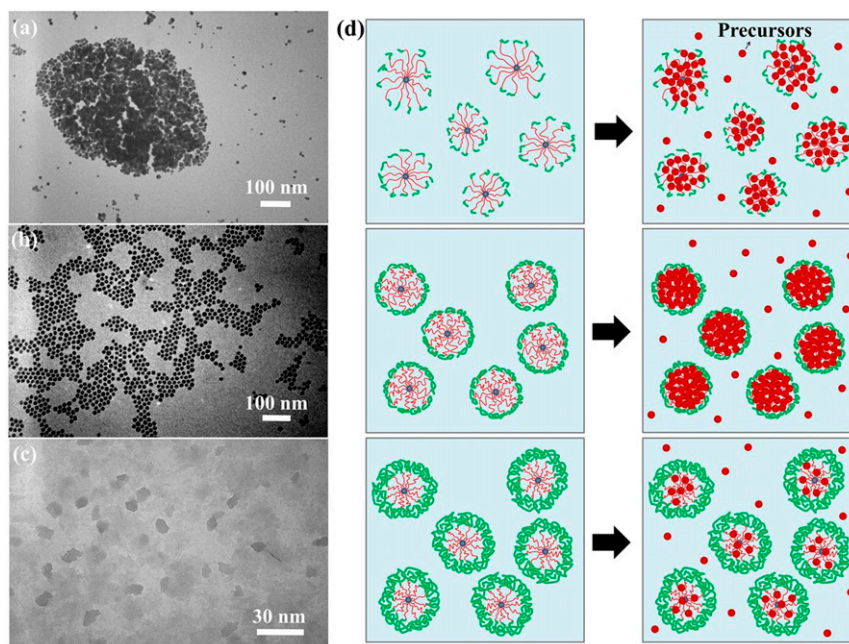
Fig. 2. Effect of MW of outer PMAMC chains on the in situ formation of Au NPs. TEM images of Au NPs formed in situ using (*A*) sample B, (*B*) sample A, and (*C*) sample C in *SI Appendix*, Table S2 as nanoreactors, respectively, in the mixed solvents of DMF and BA at the volume ratio of DMF/BA of 7/3. (*D*) Proposed mechanism for synthesis of uniform Au NPs (using sample A as nanoreactor where PMAMC has an intermediate MW, M_n; central panels) and nonuniform Au NPs (using sample B in *Upper* and sample C in *Lower* as nanoreactors, where M_n of PMAMC are relatively too small and too large, respectively) in the 7/3 DMF/BA mixed solvents.

XRD measurements confirmed that Au NPs prepared by the nanoreactor strategy were crystalline.

Light-Enabled Reversible Self-Assembly of PMAMC-Capped Au NPs. Subsequently, monodisperse hairy PMAMC-capped Au NPs with a diameter of 14.9 ± 0.3 nm were exploited as building blocks to scrutinize their light-enabled reversible self-assembly and disassembly enabled by [2 + 2] photodimerization (14) and photocleavage of coumarin moieties in PMAMC, respectively. The as-prepared PMAMC-capped Au NPs CH_2Cl_2 solution ($c =$ 8.3 μM) displayed a characteristic SPR peak at 525 nm. Interestingly, when exposing to UV light at the wavelength of 365 nm for 180 min (Fig. 3*A*; *Materials and Methods*), the SPR peak position of PMAMC-capped Au NPs continuously red-shifted from 525 to 584 nm (a total of 59-nm red shift), accompanied by the decreased intensity and increased full width at half-maximum (FWHM). The red shift and broadening of the SPR peak observed during UV irradiation resulted from the collective electromagnetic response of self-assembled Au NPs to visible light (33–35). On the other hand, the screening of Au NPs buried within the self-assembled interior limited their full illumination, and thus led to the lowered intensity of the SPR peak (33–35). It is noteworthy that when 365-nm UV irradiation was applied to polystyrene (PS)-capped Au NPs and 1-dodecanethiol (DDT)-capped Au NPs CH_2Cl_2 solutions, no appreciable changes in the SPR spectra were observed (*SI Appendix*, Figs. S15 and S16; *Materials and Methods*), unambiguously demonstrating that the self-assembly of PMAMC-capped Au NPs was arisen from the photodimerization (i.e., photo–cross-linking) of coumarin moieties in PMAMC chains capped on the Au NP surface (Fig. 4 *A–C*). The PMAMC-capped Au NPs CH_2Cl_2 solution was subsequently irradiated by 254-nm UV light for 45 min (*Materials and Methods*). Intriguingly, the SPR peak was found to blue shift from 584 to 525 nm as the UV irradiation progressed (Fig. 3*B*). There was an increase in the SPR peak intensity and a narrowing in its FWHM accordingly (Figs. 3*B* and

4*C*). Notably, compared with the photodimerization process (i.e., self-assembly of PMAMC-capped Au NPs), the speed of photocleavage process (i.e., disassembly of PMAMC-capped Au NPs) is much faster due likely to the higher energy of 254-nm UV light than the 365-nm counterpart. The light-enabled reversible self-assembly was found to depend on the concentration of PMAMC-capped Au NPs CH_2Cl_2 solution (*SI Appendix*, Figs. S17 and S18). For solutions at concentration of ≥1.0 μM, Au NPs self-assembled induced by 365-nm UV light irradiation, whereas no NP self-assembly at the concentration <1.0 μM was seen over the irradiation time. Unless otherwise specified, the concentration of PMAMC-capped Au NPs CH_2Cl_2 solution was 8.3 μM.

The color of the PMAMC-capped Au NPs CH_2Cl_2 solution was gradually varied from red to purple under 365-nm UV light irradiation and slowly recovered to its original red color upon subsequent irradiation with 254-nm UV light (*SI Appendix*, Fig. S19). It is worth noting that, during the UV irradiation process, no precipitation occurred in the solution due to the good solubility of PMAMC-capped Au NPs even in their self-assembled states (Figs. 3*A* and 4*C* and *SI Appendix*, Fig. S19*A*). This is because of the stable and permanent tethering of PMAMC chain on the surface of Au NP. As shown in Fig. 3*C*, the position of SPR peaks of PMAMC-capped Au NPs can be reversibly alternated between 525 and 584 nm triggered by 365- and 254-nm UV light irradiation, respectively, signifying a reversible assembly–disassembly cycle of PMAMC-capped Au NPs in CH_2Cl_2 due to robust repeatable photodimerization and photocleavage of PMAMC chains anchored on the surface of Au NP. The reversibility was further verified via DLS measurements after repeated light-enabled self-assembly and disassembly processes, where the sizes of self-assembled and disassembled NPs remained rather constant (*SI Appendix*, Fig. S20).

The transmission electron microscope (TEM) imaging was performed to scrutinize the evolution of light-enabled reversible self-assembly described above. The as-prepared PMAMC-capped Au NPs before UV irradiation possessed an average
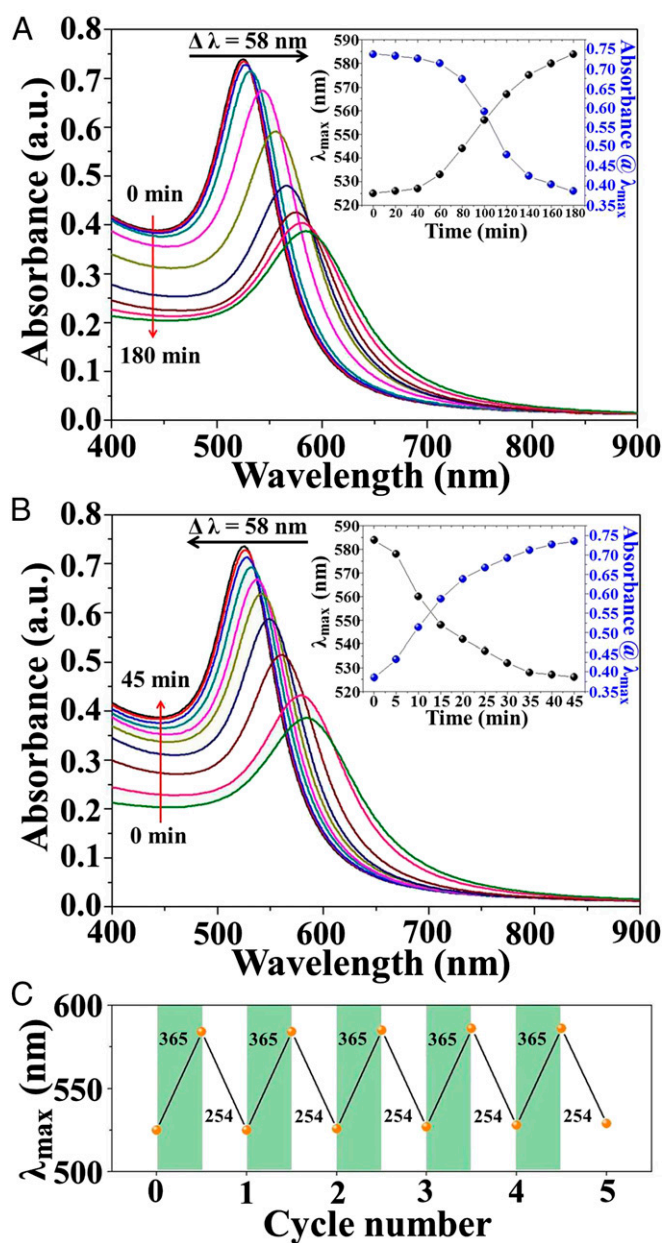
Fig. 3. Reversible optical properties of photoresponsive NPs. (A) UV–vis spectra of PMAMC-capped Au NPs CH$_2$Cl$_2$ solution (c = 8.3 μM) when irradiated with 365-nm UV light. (B) UV–vis spectra of PMAMC-capped Au NPs CH$_2$Cl$_2$ solution upon irradiation with subsequent 254-nm UV light after being exposed to 365-nm UV light for 180 min in A. (A and B, Insets) The maximum peak position λ$_{max}$ and the absorbance of the SPR peaks at λ$_{max}$ as a function of UV irradiation time. (C) Reversible photocontrol of the SPR peak position of PMAMC-capped Au NPs during the self-assembly (green bars) and disassembly (white bars) cycles upon the irradiation with 365- and 254-nm UV light, respectively.

diameter of 14.9 ± 0.3 nm. They were uniform and well dispersed without aggregation (Fig. 5A). A representative high-resolution transmission electron microscope (HRTEM) image of a single PMAMC-capped Au NP clearly showed the crystalline structure with a lattice spacing of ~0.239 nm, that is, (111) interplanar distance of the fcc Au (*SI Appendix*, Fig. S21). A size distribution histogram for PMAMC-capped Au NPs is depicted in *SI Appendix*, Fig. S22. The size distribution of these NPs is within 3% of their average size, suggesting that they are monodisperse.

Upon the use of 365-nm UV light as a trigger, the coumarin moieties in the outer PMAMC chains capped on the surface of Au NP underwent a photodimerization process (Fig. 4C). As a result, the PMAMC-capped Au NPs gradually formed large aggregates with irregular shape and varied thickness (Figs. 4C and 5 A–D). This contrasts sharply to PS-capped Au NPs and DDT-capped Au NPs with which no distinct self-assembly was seen after 365-nm UV irradiation for 24 h (Fig. 6 A, B, and D–F; the corresponding size distribution histograms for PS-capped and DDT-capped Au NPs are shown in *SI Appendix*, Figs. S23 and S24, respectively). Remarkably, upon irradiation with 254-nm UV light, the formed Au NP aggregates disassembled and eventually returned to their isolated single NP state with well-retained size and shape after 45 min (Fig. 5 E–H). It is important to note that self-assembled Au aggregates did not precipitate from CH$_2$Cl$_2$ during the photodimerization process (Fig. 3A) due to the intimately and permanently tethered PMAMC chains on their surface that rendered good solubility of Au aggregates. The dimerization degree D of PMAMC-capped Au NPs (c = 8.3 μM) upon UV irradiation can be quantified by ^{1}H-NMR and UV–vis measurements. The 365-nm UV light irradiation for 180 min yielded a D of ~74%, which decreased to ~19% upon subsequent 254-nm UV light irradiation for 45 min (*SI Appendix*, Figs. S25–S27).

Discussion

For PS-capped Au NPs, similar to their UV–vis spectra obtained by exposing to 365-nm UV light for 24 h (*SI Appendix*, Fig. S15) as discussed above, the peak position and the shape of SPR absorption of Au NPs still remained unchanged upon the subsequent 254-nm UV light irradiation for an additional 24 h (*SI Appendix*, Fig. S28). Likewise, these PS-capped NPs stayed well-dispersed during the course of UV irradiation owing to the direct
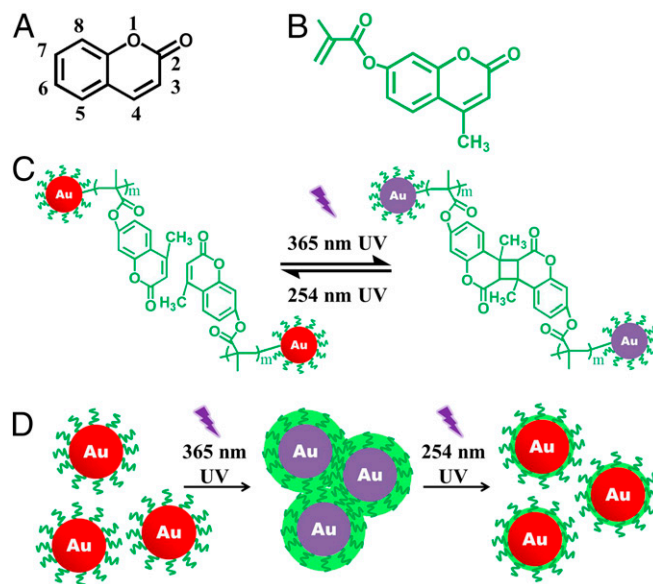

Fig. 4. Light-enabled reversible self-assembly of Au NPs intimately and permanently capped with photoresponsive polymer chains. Chemical structures of (A) coumarin and (B) MAMC (i.e., Fig. 1, *Center Right*). (C) Schematic illustration of photodimerization (photo–cross-linking) and photocleavage behaviors of PMAMC chains situated on the surface of Au NPs when subjected to 365- and 254-nm UV light irradiation, respectively. (D) Stepwise representation of light-enabled self-assembly and disassembly of PMAMC-capped Au NPs upon 365- and 254-nm UV light irradiation, respectively. The thicker green ring in D represents the complete photo–cross-linking of PMAMC chains, whereas the thinner green ring depicts the incomplete photocleavage (*SI Appendix* and *SI Appendix*, Figs. S36 and S37).
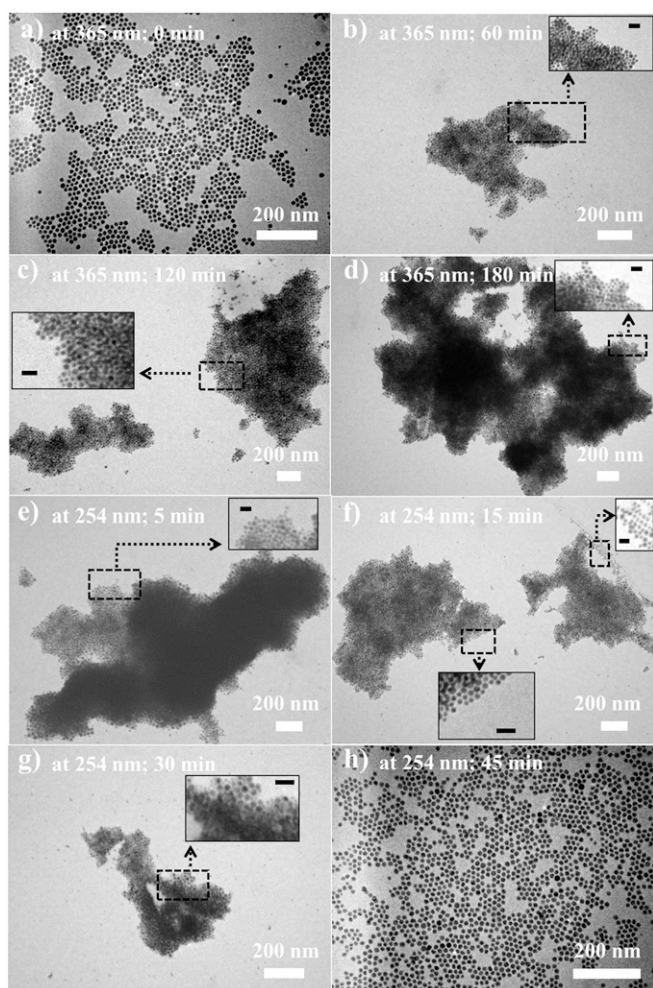
Fig. 5. Evolution of light-enabled reversible self-assembly of PMAMC-capped Au NPs with retained morphology. TEM images of PMAMC-capped Au NPs after the PMAMC-capped Au NPs CH$_2$Cl$_2$ solution (c = 8.3 μM) was exposed to (*A–D*) 365-nm UV light and (*E* and *F*) 254-nm UV light for a given time. The corresponding time-dependent UV–vis spectra are shown in Fig. 3 *A* and *B*, respectively. It is worth noting that images (*E* and *F*) were obtained by subsequent 254-nm UV light irradiation on the PMAMC-capped Au NPs CH$_2$Cl$_2$ solution after it was previously irradiated by 365-nm UV light for 24 h. The 365-nm UV exposure times are (*A*) t = 0 min, (*B*) t = 60 min, (*C*) t = 120 min, and (*D*) t = 180 min. The 254-nm UV exposure times (*E*) t' = 5 min, (*F*) t' = 15 min, (*G*) t' = 30 min, and (*H*) t' = 45 min. (Scale bars: *Insets*, 50 nm.)

and permanent tethering of outer PS chains (*SI Appendix*, Scheme S3*A*S3*A*), as clearly evidenced in TEM images (Fig. 6) and digital images (*SI Appendix*, Fig. S29). It is well known that Au NPs possess photothermal effect. To evaluate the possible role of photothermal effect, control experiments were performed (*SI Appendix*, Figs. S30 and S31). The results demonstrated that photothermal effect cannot account for light-enabled NP self-assembly.

As noted above, Au–SH bond is unstable when subjected to UV light irradiation (16, 22). This was further verified in our study. DDT-capped Au NPs with an average diameter of 14.8 ± 3 nm were prepared (*Materials and Methods*; nearly same NP size as PMAMC-capped and PS-capped Au NPs). As –SH ligand is a strong capping ligand, the diameter of Au NPs prepared by Brust method and its derived approaches is often less than 5 nm (36). To this end, DDT-capped Au NPs were obtained via a post-synthesis treatment from the preformed 14.8 ± 3-nm oleylamine (OAm)-capped Au NPs (i.e., ligand exchange of original OAm

with DDT). Subsequently, these DDT-capped Au NPs were dissolved in CH$_2$Cl$_2$ and irradiated by 365- and 254-nm UV light, respectively. As discussed above, when 365-nm UV light was applied for 24 h, the SPR absorption did not change much (only with a small broadening in FWHM; *SI Appendix*, Fig. S16). Moreover, the size distribution and morphology of DDT-capped Au NPs were also almost the same with a slight tendency of aggregation (Fig. 6 *D–F*), and no precipitation was seen during the irradiation process (*SI Appendix*, Fig. S32, *Center* digital images). In sharp contrast, under 254-nm UV light irradiation, the DDT-capped Au NPs progressively formed irregular aggregates, and no individual Au NPs can be observed (Fig. 6 *G–I*). Meanwhile, the characteristic SPR peak disappeared (*SI Appendix*, Fig. S33). Finally, the aggregates precipitated to the bottom from CH$_2$Cl$_2$ (*SI Appendix*, Fig. S32, *Right*, digital images). Taken together, it is clear that the Au–SH bond was destroyed (i.e., the DDT ligands were dissociated from the Au NP surface) under 254-nm UV light irradiation for a short period of time. This dissociation is caused by photooxdization of thiol to sulfonate groups (16), leading to the agglomeration of Au NPs due to markedly reduced bonding ability of sulfonate groups to Au NPs. Although 365-nm UV light has relatively low energy and did not induce the oxidation of DDT, the thermal desorption of DDT may occur due to local overheating, which can also potentially break the Au–SH bond (16). Since the photo-oxidation of surface ligand is dominated by oxygen with varied solubility in solvent, the photoresponsive capability (i.e., NP self-assembly) for Au NPs capped with SH-terminated ligands relies on the surrounding solvent (37–39). However, because of no Au–SH bonding in PMAMC-capped Au NPs prepared by the nanoreactor strategy, there was no notable solvent effect on the Au NP self-assembly (*SI Appendix*, Fig. S34). Clearly, thiol ligand-capped Au NPs do not stand out as robust building blocks for light-enabled reversible self-assembly when UV light is employed as a stimulus (*SI Appendix*, Scheme S3*B*).

We also compared the use of linear diblock copolymer with star-like diblock copolymer as nanoreactors on Au NPs synthesis. Linear PAA-*b*-PMAMC diblock copolymer with similar MW and ratio of two blocks as those of the star-like block copolymer (i.e., *SI Appendix*, Table S2, sample A) was also prepared by sequential ATRP (*SI Appendix*, Table S4). This linear diblock copolymer was then used as a nanoreactor to synthesize Au nanocrystals under the same experimental conditions as star-like diblock copolymer (*SI Appendix*, Scheme S4). It is clear that when linear PAA-*b*-PMAMC was used as the nanoreactor, the precipitates that are likely a mixture of Au and unreacted precursors quickly formed on the bottom of vial (*SI Appendix*, Fig. S35, *Inset*). In contrast, the solution remained homogeneous without any precipitation even under UV irradiation in the case of Au NPs produced by capitalizing on star-like PAA-*b*-PMAMC as the nanoreactor (*SI Appendix*, Fig. S19). The TEM measurement showed that the precipitates are composed of large irregular structures (*SI Appendix*, Fig. S35). In addition, the TEM sample prepared from the supernatant was also characterized, and no inorganic structures were observed.

Light-enabled reversible self-assembly with cavities between adjacent NPs can be exploited as unique and efficient nanocarriers to deliver and release various guest molecules. In this context, Rhodamine B (RhB) (a fluorescent dye) and PMAMC-capped Au NPs were employed as the model guest molecule and the self-assembled nanocarriers, respectively, to demonstrate the capability of compound release. As-prepared PMAMC-capped Au NPs CH$_2$Cl$_2$ solutions (i.e., without self-assembly; c = 8.3 μM) and RhB dyes were mixed (Fig. 7*A*, first column) and exposed to 365-nm UV irradiation for 180 min to load RhB. As 365-nm UV light triggered the photodimerization of PMAMC blocks, PMAMC-capped Au NPs self-assembled and RhB molecules were loaded in the cavities within the self-assembled
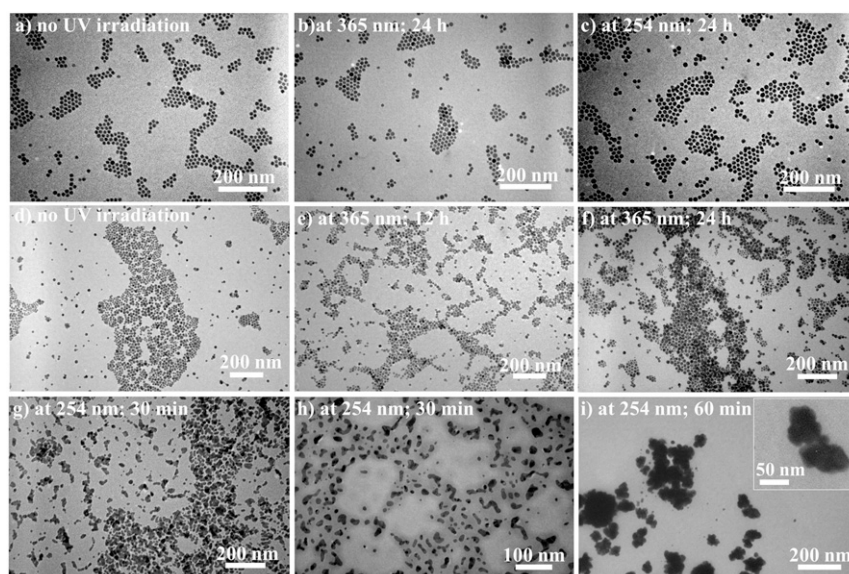
Fig. 6. Morphological evolutions of Au NPs either permanently capped with nonphotoresponsive polymers or dynamically capped with small molecules. TEM images of (*A*) as-prepared PS-capped Au NPs before UV light irradiation, and (*B* and *C*) PS-capped Au NPs after 365- and 254-nm UV light irradiation, respectively, for 24 h. It is notable that image (*C*) was obtained by irradiating the PS-capped Au NPs CH₂Cl₂ solution with 254-nm UV light for an additional 24 h after it was previously exposed to 365-nm UV light for 24 h. TEM images of (*D*) as-prepared DDT-capped Au NPs before UV light irradiation, and (*E* and *F*; and *G–I*) DDT-capped Au NPs after 365-nm (for 24 h) and 254-nm (for 60 min) UV light irradiation, respectively. Notably, images (*G–I*) were obtained by irradiating the DDT-capped Au NPs CH₂Cl₂ solution with 254-nm UV light for an additional 60 min after it was previously exposed to 365-nm UV light for 24 h. A close-up in *Inset* shows the agglomeration of Au nanocrystals with no observable, individually isolated NPs.

Au NPs during self-assembly process (Fig. 7*A*, second column). Then, UV light was removed and a poor solvent of PMAMC (i.e., methanol) was added to the solution. Consequently, RhB dyes were trapped within the self-assembled Au NPs due to the collapsed outer PMAMC chains (Fig. 7*A*, third column). After collection and washing by centrifugation to remove free dyes, self-assembled Au NPs loaded with RhB molecules were redispersed in CH₂Cl₂ with UV irradiation at 254 nm. As CH₂Cl₂ rendered PMAMC chains to recover their extended conformation in conjunction with the 254-nm UV light-induced photocleavage of PMAMC block, which led to disassembly of PMAMC-capped Au NPs, RhB dyes diffused into the surrounding CH₂Cl₂ (Fig. 7*A*, fourth column). We note that methanol was added to the system at different desired times, followed by centrifugation to obtain the supernatant. As RhB has a characteristic absorption peak located at ∼550 nm, the release behavior of RhB molecules in this process (denoted release process R1) can be readily scrutinized by monitoring the UV–vis spectra of the supernatants at different irradiation times with 254-nm UV light. As shown in Fig. 7*B*, the absorption peak intensity progressively increased when self-assembled Au NPs were irradiated with 254-nm UV light as a result of steady release.

In addition to the release process R1, control experiments (R2–R5) were also carried out under the same conditions, except for release process R2, as-prepared PMAMC-capped Au NPs were first irradiated by 365-nm UV light for 180 min and then mixed with RhB molecules for 180 min with no UV light irradiation (*SI Appendix*, Fig. S39*A* and Scheme S6*B*); for release process R3, the 254-nm UV light was off when releasing RhB molecules (*SI Appendix*, Fig. S39*B* and Scheme S6*C*); for release process R4, as-prepared PMAMC-capped Au NPs were mixed with RhB molecule under 365-nm UV light irradiation for 180 min and subsequent 254-nm UV light irradiation for 45 min prior to the dye release; and for release process R5, as-prepared PMAMC-capped Au NPs were mixed with RhB molecules without UV irradiation.

The release kinetics of dyes in these release processes (R1–R5) was summarized in Fig. 7*C*. A high concentration gradient of RhB molecules from inside self-assembled Au NPs to the surrounding solvent triggered the large initial release rate. Then, the release rate decreased as the concentration gradient gradually became smaller. The number of released RhB dyes in release processes R2 and R3 were ∼40% and 15% of that in release process R1 (Fig. 7*C*, curves R1–R3), revealing that the encapsulation and release rates can be greatly enhanced via such light-enabled reversible self-assembly and disassembly, respectively. Such markedly improved encapsulation and release rates using PMAMC-capped Au NPs clearly overcome the diffusion limitation often encountered in other nanocarrier systems (e.g., zeolite, etc.) (10). When there presents no reversible self-assembly (release processes R4 and R5), almost no release occurred (Fig. 7*C*, curves R4–R5).

Moreover, as light can be remotely applied to the system, the release capability can be controlled by the intermittent UV irradiation at 254 nm, even after the beginning of release. Therefore, stepwise controlled release was performed in the same way as release process R1 except performing 254-nm UV light on/off cycles every 10 min (denoted release process R6; Fig. 7*D*). The amount of released RhB dyes continuously increased upon 254-nm UV light irradiation and the release almost terminated once the UV light was off but remaining the switchable ability in the following light on/off cycles. This result clearly substantiated that the release capability can be precisely controlled using such light-enabled reversible self-assembly. This capability together with tunable optical properties is of significance in advancing the applications in catalysis, nanosensors, etc.

In summary, we developed a viable star-like block copolymer nanoreactor strategy for in situ crafting of monodisperse stable hairy plasmonic NPs intimately and permanently functionalized with photoresponsive polymers. As demonstrated in this work, the rationally designed amphiphilic star-like PAA-*b*-PMAMC diblock copolymers confer the formation of photoresponsive PMAMC-capped Au NPs. The size of Au NPs and the length of
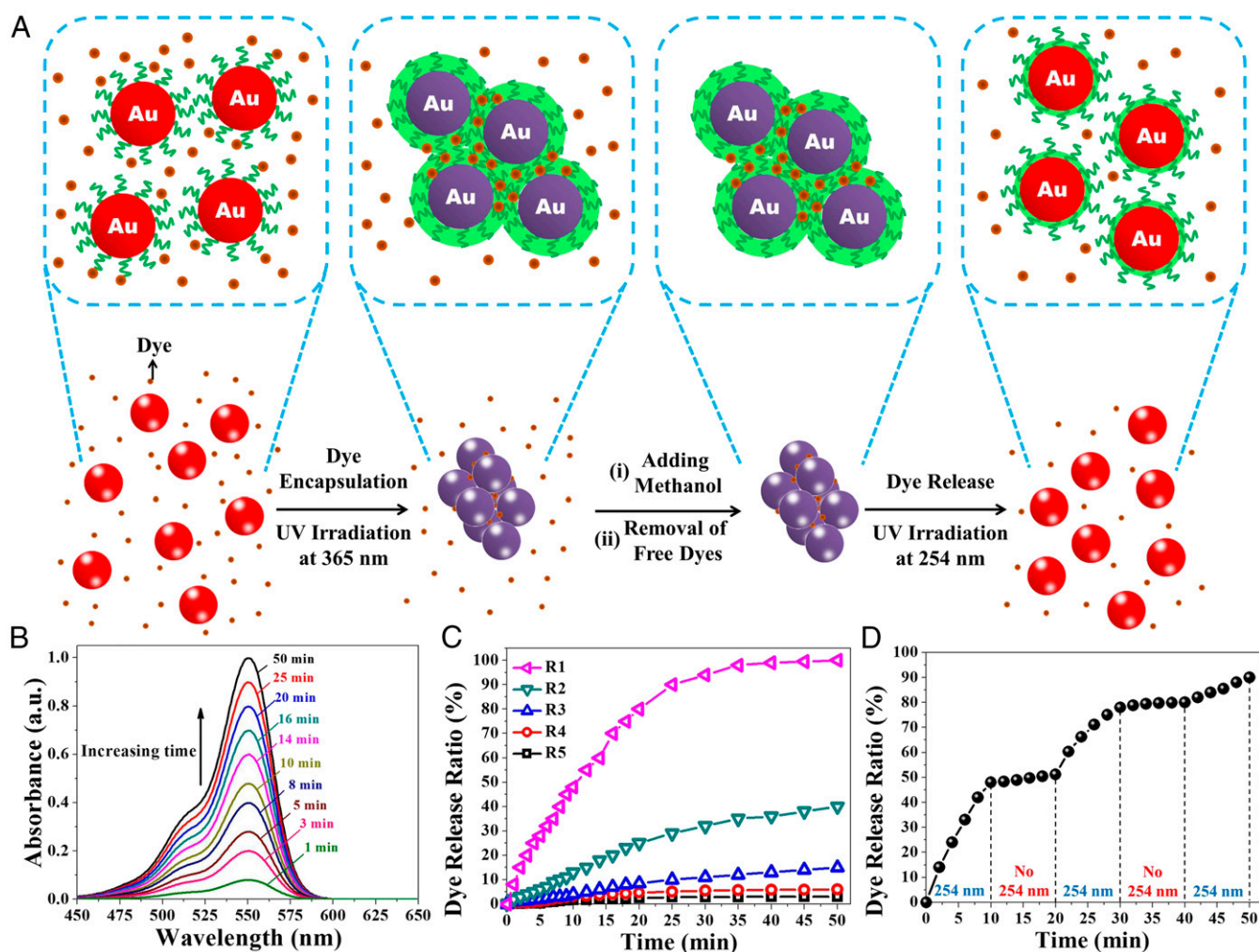
Fig. 7. Encapsulation and release of a model dye using light-enabled reversible self-assembly of PMAMC-capped Au NPs. (*A*) Stepwise representation of encapsulation and release of RhB molecules by capitalizing on the light-enabled reversible self-assembly of PMAMC-capped Au NPs ($c = 8.3$ μM) in release process R1. (*B*) UV–vis spectra of released RhB molecules in release process R1 as a function of 254-nm UV light irradiation time. (*C*) Release kinetics of RhB molecules in release processes R1–R5 at various times of 254-nm UV light irradiation. (*D*) Controlled release of RhB molecules in release process R6 with multiple 254-nm UV light on/off cycles. The release ratio as a function of time was determined from the absorbance intensity at 550 nm of supernatant with the saturated intensity in R1 taken as 100%.

photoresponsive PMAMC hairs situated on the Au NP surface can be readily tuned by controlling the ATRP time of the respective PAA and PMAMC blocks. Remarkably, because of stable and permanent connection between PMAMC chains and Au NP rendered by the original covalent bonding between PAA and PMAMC chains, PMAMC-capped Au NPs can be reversibly and reliably self-assembled and disassembled on demand using UV light of different wavelengths, as evidenced by tunable SPR absorption of Au NPs and the reversible transformation of Au NPs between their dispersed and aggregated states. This contrasts starkly with small molecular DDT-capped Au NPs, which experience no change in the SPR property and the precipitation of Au NPs upon UV irradiation, despite the semicovalent bonding between –SH and Au. These photoresponsive NPs may stand out as effective and smart nanocarriers. By selecting proper precursors, a wide range of other functional hairy NPs (e.g., magnetic, ferroelectric, upconversion, and semiconducting) capped with the exactly same photoresponsive polymer (i.e., PMAMC hair) can be readily produced, thereby dispensing with the need for cumbersome synthesis of ligands with specific end groups for targeted attachment on these NPs as in copious past

work. We envision that the star-like block copolymer nanoreactor strategy can be readily extended to craft virtually unlimited types of stable hairy dual-functional polymer-capped NPs (for example, water-soluble, oil-soluble, conductive, ferroelectric, temperature-sensitive, pH-sensitive, light-responsive polymer-capped metallic, magnetic, ferroelectric, upconversion, and semiconducting NPs) and their assemblies for exploring and comparing their potentially intriguing self-assembly and crystallization behaviors as well as many practical applications in optics, optoelectronics, magnetic materials and devices, and sensors, among other areas. As such, they present an enticing prospect for future studies.

Materials and Methods

acetic acid overnight, then washed with ethanol and diethyl ether successively, and dried under vacuum. tBA (98.0%; Sigma-Aldrich), anisole (99.0%; TCI America), methyl ethyl ketone (MEK) (99.9%; Fisher Scientific), and DMF (99.9%; Fisher Scientific) were dried over calcium hydride (CaH$_2$) and distilled under reduced pressure before use. Styrene (St) (≥99.0%; Sigma-Aldrich) was washed with 10% NaOH aqueous solution and then water, sequentially dried over anhydrous MgSO$_4$ and CaH$_2$, and finally distilled under reduced pressure before use. All other reagents were purified by common purification procedures.

Synthesis of MAMC Monomer. The MAMC monomer (Fig. 1, *Center Right*) was synthesized according to the literature (40). Briefly, 12.0 g of 7-hydroxy-4-methylcoumarin (Fig. 1, *Center Left*) was dissolved in 192 mL of NaOH aqueous solution (0.5 M) at room temperature. After adding 150 mL of CHCl$_3$, the solution was then cooled to 5 °C under vigorous stirring. A total of 7.1 g of methacryloyl chloride (Fig. 1, *Center Middle*) was injected into the solution to start the reaction. The reaction was terminated after 1 h by evaporating CHCl$_3$ during which the solid gradually precipitated in water. The raw white solid was collected, purified by recrystallization in acetone, and dried under vacuum at 45 °C for 12 h, yielding pure MAMC monomer ready for the following polymerization.

Synthesis of Star-Like P*t***BA Homopolymer Terminated with Bromine Groups (i.e., Star-Like P***t***BA-Br).** Heptakis[2,3,6-tri-*O*-(2-bromo-2-methylpropionyl)]-β-cyclodextrin (denoted 21Br-β-CD) was first synthesized according to procedures in our previous work (26, 27). Star-like P*t*BA-Br (Fig. 1, *Upper Right*) was prepared by ATRP of *t*BA monomer in MEK using 21Br-β-CD as the macroinitiator (Fig. 1, *Upper Center*) with CuBr/PMDETA as the cocatalyst. Typically, CuBr (35.0 mg), PMDETA (85.0 mg), 21Br-β-CD (50 mg), and *t*BA (21 mL) dissolved in MEK (21 mL) were placed in an argon-purged ampule and vacuumed by three freeze–pump–thaw cycles in liquid nitrogen, followed by a final argon purge. The ampule was then sealed and immersed in an oil bath at 60 °C. The reaction was terminated by placing the ampule in liquid nitrogen after 10 h. After dilution with THF, the solvent was then passed through a column filled with neutral alumina to remove the copper salts and subsequently purified through fractional precipitation using methanol/water (vol/vol of 1/1) as the precipitator. The product was collected and dried at 40 °C in a vacuum oven for 48 h.

Synthesis of Star-Like P*t***BA-*b*-PMAMC Diblock Copolymer.** Briefly, an argon-purged ampule charged with the reaction mixture [MAMC/star-like P*t*BA (i.e., Br in P*t*BA macroinitiator)/copper bromide/PMDETA of 800:1:1:2 (molar ratio) in DMF (1 g of MAMC in 5 mL of solvent)] was vacuumed by three freeze–pump–thaw cycles in liquid nitrogen. After reaction at 65 °C for 24 h, the mixture was quenched by dipping the ampule in liquid nitrogen. The raw product was diluted with CH$_2$Cl$_2$ and then passed through a column of neutral alumina to remove the copper salts and subsequently purified by fractional precipitation using methanol/water (vol/vol of 1/1) as the precipitator. The yielded star-like P*t*BA-*b*-PMAMC (Fig. 1, *Lower* fourth panel) was finally collected and dried at 40 °C in vacuum oven for 48 h.

Synthesis of Star-Like P*t***BA-*b*-PS Diblock Copolymer.** Briefly, the reaction mixture with a molar ratio of styrene/star-like P*t*BA (i.e., Br in P*t*BA macroinitiator)/copper bromide/PMDETA of 800:1:1:2 in anisole (1 g of St in 1 mL solvent) was placed in an argon-purged ampule and vacuumed by three freeze–pump–thaw cycles in liquid nitrogen. The polymerization was maintained at 90 °C for 24 h and quenched by placing the ampule in liquid nitrogen. The solution was diluted with THF and then passed through a column of neutral alumina to remove the copper salts and subsequently purified by fractional precipitation using methanol/water (vol/vol of 1/1) as the precipitant. The resulting star-like P*t*BA-*b*-PS was collected and dried at 40 °C in a vacuum oven for 48 h.

Synthesis of Star-Like PAA-*b*-PMAMC Diblock Copolymer by Hydrolysis. Star-like PAA-*b*-PMAMC diblock copolymers were obtained by hydrolyzing *tert*-butyl ester groups of P*t*BA blocks in star-like P*t*BA-*b*-PMAMC diblock copolymers (Fig. 1, *Lower* fourth panel). Briefly, 300 mg of star-like P*t*BA-*b*-PMAMC was completely dissolved in 30 mL of CHCl$_3$, and 3 mL of TFA was then added to start the hydrolysis. The reaction solution was stirred at room temperature for 24 h. After hydrolysis, the resulting star-like PAA-*b*-PMAMC diblock copolymers were gradually precipitated in CHCl$_3$. The final product was collected, washed with CHCl$_3$, and thoroughly dried in a vacuum oven at 50 °C overnight.

Synthesis of Star-Like PAA-*b*-PS Diblock Copolymer by Hydrolysis. The hydrolysis procedure to obtain star-like PAA-*b*-PS diblock copolymers was similar to that performed for star-like PAA-*b*-PMAMC diblock copolymers. Briefly, after completely dissolving 300 mg of star-like P*t*BA-*b*-PS in 30 mL of CHCl$_3$, 3 mL of TFA was added to start the hydrolysis. After the reaction solution was stirred at room temperature for 24 h, the resulting amphiphilic star-like PAA-*b*-PS diblock copolymers were gradually precipitated in CHCl$_3$. The final product was filtered, washed with CHCl$_3$, and thoroughly dried in a vacuum oven at 50 °C overnight.

Synthesis of PMAMC-Capped Au NPs. By capitalizing on star-like PAA-*b*-PMAMC diblock copolymers as nanoreactors, PMAMC-capped Au NPs were prepared. The reaction is performed in the DMF/BA mixed solvents. As DMF is a good solvent for both PAA and PMAMC blocks while BA is a good solvent for PAA blocks only, star-like PAA-*b*-PMAMC forms a stable spherical unimolecular micelle with the expanded inner PAA chains and the collapsed outer PMAMC chains. The Au precursors (HAuCl$_4$·3H$_2$O) are preferentially incorporated in the space filled with inner hydrophilic PAA blocks of star-like PAA-*b*-PMAMC diblock copolymers due to the strong coordination interaction between the metal moieties of HAuCl$_4$·3H$_2$O and the carboxyl groups (−COOH) of PAA and the formation of structurally stable spherical unimolecular micelle noted above, thereby resulting in the nucleation and growth of PMAMC-capped Au NPs. In a typical process, 10 mg of star-like PAA-*b*-PMAMC was dissolved in 10 mL of mixed solvents of DMF and BA at a volume ratio of DMF/BA of 7/3 at room temperature, followed by the addition of precursors. To maximize the precursor loading in the compartment occupied by PAA blocks, 10 times molar excess of precursors to acrylic acid (AA) units in PAA blocks was employed. To ensure that all chemicals except the reducer were fully dissolved, the mixture was stirred under argon for a week. Subsequently, 2.5 times of the reducer (i.e., TBAB) to the precursors (molar ratio) was added into the reaction system. The reaction was then performed at 60 °C under argon. After 2 h, the solution was centrifuged at $95 \times g$ to remove the precipitates and purified by ultracentrifugation several times using CH$_2$Cl$_2$ as solvent and ethanol as precipitant to remove unreacted precursors and the mixed solvents, yielding Au NPs intimately and stably capped with PMAMC. The average diameters of PMAMC-capped Au NPs are 14.9 ± 0.3 and 9.8 ± 0.5 nm using sample A and sample E in *SI Appendix*, Table S2, respectively. Photo–cross-linking (i.e., self-assembly) or photocleavage (i.e., disassembly) reactions of PMAMC-capped Au NPs were performed by alternative irradiation with a mercury low-pressure UV lamp at 365-nm (25 W) or 254-nm (4 W), respectively, for certain periods of time. Unless otherwise specified, PMAMC-capped Au NPs for the UV irradiation studies are those with a diameter of 14.9 ± 0.3 nm crafted using sample A in *SI Appendix*, Table S2.

Synthesis of PS-Capped Au NPs. As our star-like block copolymer strategy has the ability to craft a rich variety of inorganic NPs intimately and stably capped with different functional polymers, we also synthesized PS-capped Au NPs with an average diameter of 14.8 ± 0.4 nm using star-like PAA-*b*-PS diblock copolymers as nanoreactors. We note that the diameter of PS-capped Au NPs (used as control) is nearly the same as that of PMAMC-capped Au NPs for better comparison in the light-enabled reversible self-assembly study. Typically, the mixed solvents, precursors, and reducer as well as the formation mechanism are the same as in the synthesis of PMAMC-capped Au NPs described above except the volume ratio of DMF to BA is changed to 9/1 to obtain monodisperse PS-capped Au NPs due to the different solubility of PS and PMAMC in the mixed DMF/BA solvents. The molar ratio of AA units in PAA blocks to precursors was 1:10 to maximize the loading of precursors into the PAA compartment. Likewise, the mixture solution (without the reducer TBAB) was stirred under argon for a week at room temperature to completely dissolve all chemicals. Subsequently, a 2.5-time (molar ratio) of TBAB to the precursors was added into the mixture. The reaction was then performed at 60 °C under argon. After 2 h, the solution was centrifuged at $95 \times g$ to remove the precipitates and purified by ultracentrifugation for several times using toluene as solvent and ethanol as precipitant to remove unreacted precursor and mixed solvents, yielding Au NPs intimately and stably capped with PS.

Synthesis of Thiol-Capped Au NPs. Thiol-capped Au NPs synthesized by Brust method and its derived methods often possess a limited size (less than 5 nm) as thiol is a strong ligand and suppresses the growth of nanocrystals (36). To prepare thiol-capped Au NPs with a diameter of ~15 nm that can be used as control for comparison with PMAMC-capped Au NPs of similar size (14.9 ± 0.3 nm) in the light-enabled reversible self-assembly study, weak ligand OAm-capped Au NPs were first synthesized, followed by ligand exchange

with strong ligand DDT. OAm-capped Au NPs with a diameter of 14.8 ± 3 nm were synthesized according to the literature (41). Briefly, 1 mL of toluene containing 50 mg of HAuCl$_4$·3H$_2$O and 1.2 mL of OAm was added to a boiling solution containing 2.09 mL of OAm and 49 mL of toluene under stirring. The solution was then cooled down to room temperature after 2 h, and purified by ultracentrifugation with toluene as solvent and ethanol as precipitant for several times to remove any remaining precursors and the mixed solvents. The as-capped OAm-capped Au NPs were dispersed in 10 mL of toluene and mixed with 25 mg of DDT (in large excess compared with NPs). The mixture was stirred vigorously for 24 h and purified by ul-tracentrifugation with toluene as solvent and ethanol as precipitant for several times to remove excess DDT and the mixed solvents, yielding DDT-capped Au NPs.

Encapsulation and Release of Dyes. A simple, general process was developed to encapsulate RhB dye as a model guest molecule by capitalizing on light-enabled reversible self-assembly of PMAMC-capped Au NPs. Taking release process R1 as an example, PMAMC-capped Au NPs CH$_2$Cl$_2$ solution (1.5 mL, 8.3 μM) was mixed with 10.5 mg of RhB. After stirring under 365-nm UV light for 180 min, 5.0 mL of methanol was added to the mixture. The self-assembled Au NPs loaded with RhB were collected by centrifugation at 4,000 × g and washed with methanol (1.0 mL) for several times until the supernatant absorbance at 550 nm in UV–vis spectrum was less than 0.01. To explore the dye release behavior, the obtained self-assembled RhB-loaded Au NPs were redispersed in 1.5 mL of CH$_2$Cl$_2$ under 254-nm UV light. At desired times, 5.0 mL of methanol was added to the system, followed by centrifugation at 4,000 × g to yield the supernatant. The number of RhB dyes released from the system was evaluated by monitoring the 550-nm supernatant absorbance at different times.

Characterizations. The number average MW (M_n) and PDI of as-prepared polymers were determined by gel permeation chromatography (GPC) equipped with a Waters 1515 system at 50 °C. A series of monodisperse polystyrene were used as the standard samples with DMF/LiBr as the eluent at a flow rate of 1.0 mL/min to calibrate the GPC. Proton NMR (^{1}H NMR) spectra were measured on a Varian VXR-300 spectroscope in which CDCl$_3$ and d$_7$-DMF were used as solvents.

The morphology and size distribution of PMAMC-capped Au, PS-capped Au, DDT-capped Au NPs were examined by TEM (JEOL 100; operated at 100 kV) and HRTEM (TECNAIG2 F30; operated at 300 kV). TEM samples were prepared by drop-casting a dilute NP solution onto a 300 mesh carbon-coated copper TEM grid under ambient condition. Mercury low-pressure UV lamps at 365 nm (25 W) or 254 nm (4 W) were used for the photo–cross-linking (i.e., self-assembly) or photocleavage (i.e., disassembly) reactions of Au NPs capped with different ligands (PMAMC-capped Au NPs, PS-capped Au, and DDT-capped Au NPs), respectively. The temperature increase of the solvents after UV irradiation can be ignored due to the heat dissipation in the fume hood. The plasmonic properties of Au NPs were recorded by UV–vis spectroscopy (Varian; UV–vis–NIR spectrophotometer; Cary 5000). DLS data were obtained using laser light-scattering spectrometer (Malvern Autosizer 4700) at 25 °C. The crystalline structures of Au NPs were investigated by XRD (X'pert PRO).

1. Grzelczak M, Vermant J, Furst EM, Liz-Marzán LM (2010) Directed self-assembly of nanoparticles. *ACS Nano* 4:3591–3605.
2. Yavuz CT, et al. (2006) Low-field magnetic separation of monodisperse Fe$_3$O$_4$ nano-crystals. *Science* 314:964–967.
3. Choi Y, Ho NH, Tung CH (2007) Sensing phosphatase activity by using gold nano-particles. *Angew Chem Int Ed Engl* 46:707–709.
4. Mirkin CA, Letsinger RL, Mucic RC, Storhoff JJ (1996) A DNA-based method for ra-tionally assembling nanoparticles into macroscopic materials. *Nature* 382:607–609.
5. Jiang X, Brinker CJ (2006) Aerosol-assisted self-assembly of single-crystal core/nano-porous shell particles as model controlled release capsules. *J Am Chem Soc* 128:4512–4513.
6. Zhang K, Zhu X, Jia F, Auyeung E, Mirkin CA (2013) Temperature-activated nucleic acid nanostructures. *J Am Chem Soc* 135:14102–14105.
7. Strozyk MS, Chanana M, Pastoriza-Santos I, Pérez-Juste J, Liz-Marzán LM (2012) Protein/polymer-based dual-responsive gold nanoparticles with pH-dependent ther-mal sensitivity. *Adv Funct Mater* 22:1436–1444.
8. Nie Z, et al. (2007) Self-assembly of metal-polymer analogues of amphiphilic triblock copolymers. *Nat Mater* 6:609–614.
9. Das S, et al. (2013) Dual-responsive nanoparticles and their self-assembly. *Adv Mater* 25:422–426.
10. Zhao H, et al. (2016) Reversible trapping and reaction acceleration within dynamically self-assembling nanoflasks. *Nat Nanotechnol* 11:82–88.
11. Kundu PK, et al. (2015) Light-controlled self-assembly of non-photoresponsive nanoparticles. *Nat Chem* 7:646–652.
12. Klajn R, Browne KP, Soh S, Grzybowski BA (2010) Nanoparticles that "remember" temperature. *Small* 6:1385–1387.
13. Jochum FD, Theato P (2013) Temperature- and light-responsive smart polymer ma-terials. *Chem Soc Rev* 42:7468–7483.
14. Trenor SR, Shultz AR, Love BJ, Long TE (2004) Coumarins in polymers: From light harvesting to photo-cross-linkable tissue scaffolds. *Chem Rev* 104:3059–3077.
15. Bokern S, et al. (2011) Precisely designed gold nanoparticles by surface polymeriza-tion—artificial molecules as building blocks for novel materials. *Adv Funct Mater* 21:3753–3759.
16. Love JC, Estroff LA, Kriebel JK, Nuzzo RG, Whitesides GM (2005) Self-assembled monolayers of thiolates on metals as a form of nanotechnology. *Chem Rev* 105:1103–1169.
17. Shiraishi Y, et al. (2014) Spiropyran-modified gold nanoparticles: Reversible size control of aggregates by UV and visible light irradiations. *ACS Appl Mater Interfaces* 6:7554–7562.
18. Grzelczak M, Liz-Marzán LM (2014) Exploiting hydrophobic interactions at the nanoscale. *J Phys Chem Lett* 5:2455–2463.
19. Housni A, Zhao Y, Zhao Y (2010) Using polymers to photoswitch the aggregation state of gold nanoparticles in aqueous solution. *Langmuir* 26:12366–12370.
20. Shiraishi Y, et al. (2013) Light-triggered self-assembly of gold nanoparticles based on photoisomerization of spirothiopyran. *Angew Chem Int Ed Engl* 52:8304–8308.
21. Ling D, Hackett MJ, Hyeon T (2014) Surface ligands in synthesis, modification, as-sembly and biomedical applications of nanoparticles. *Nano Today* 9:457–477.
22. Park J, Joo J, Kwon SG, Jang Y, Hyeon T (2007) Synthesis of monodisperse spherical nanocrystals. *Angew Chem Int Ed Engl* 46:4630–4660.
23. Xu H, et al. (2015) A general route to nanocrystal kebabs periodically assembled on stretched flexible polymer shish. *Sci Adv* 1:e1500025.
24. Pang X, He Y, Jung J, Lin Z (2016) 1D nanocrystals with precisely controlled dimen-sions, compositions, and architectures. *Science* 353:1268–1272.
25. Pang X, Zhao L, Han W, Xin X, Lin Z (2013) A general and robust strategy for the synthesis of nearly monodisperse colloidal nanocrystals. *Nat Nanotechnol* 8:426–431.
26. Pang X, Zhao L, Akinc M, Kim JK, Lin Z (2011) Novel amphiphilic multi-arm, star-like block copolymers as unimolecular micelles. *Macromolecules* 44:3746–3752.
27. Pang X, Zhao L, Feng C, Lin Z (2011) Novel amphiphilic multiarm, starlike coil–Rod diblock copolymers via a combination of click chemistry with living polymerization. *Macromolecules* 44:7176–7183.
28. Chen Y, et al. (2017) Hairy uniform permanently ligated hollow nanoparticles with precise dimension control and tunable optical properties. *J Am Chem Soc* 139:12956–12967.
29. Jiang B, Pang X, Li B, Lin Z (2015) Organic-inorganic nanocomposites via placing monodisperse ferroelectric nanocrystals in direct and permanent contact with fer-roelectric polymers. *J Am Chem Soc* 137:11760–11767.
30. He M, et al. (2016) Monodisperse dual-functional upconversion nanoparticles enabled near-infrared organolead halide perovskite solar cells. *Angew Chem Int Ed Engl* 55:4280–4284.
31. Chen Y, et al. (2016) Precisely size-tunable monodisperse hairy plasmonic nano-particles via amphiphilic star-like block copolymers. *Small* 12:6714–6723.
32. Matyjaszewski K, Tsarevsky NV (2009) Nanostructured functional materials prepared by atom transfer radical polymerization. *Nat Chem* 1:276–288.
33. Storhoff JJ, et al. (2000) What controls the optical properties of DNA-linked gold nanoparticle assemblies? *J Am Chem Soc* 122:4640–4650.
34. Lazarides AA, Schatz GC (2000) DNA-linked metal nanosphere materials: Structural basis for the optical properties. *J Phys Chem B* 104:460–467.
35. Jin R, Wu G, Li Z, Mirkin CA, Schatz GC (2003) What controls the melting properties of DNA-linked gold nanoparticle assemblies? *J Am Chem Soc* 125:1643–1654.
36. Templeton AC, Wuelfing WP, Murray RW (2000) Monolayer-protected cluster mole-cules. *Acc Chem Res* 33:27–36.
37. Aldana J, Wang YA, Peng X (2001) Photochemical instability of CdSe nanocrystals coated with hydrophilic thiols. *J Am Chem Soc* 123:8844–8850.
38. Battino R, Rettich TR, Tominaga T (1983) The solubility of oxygen and ozone in liq-uids. *J Phys Chem Ref Data* 12:163–178.
39. He H, Feng M, Chen Q, Zhang X, Zhan H (2016) Light-induced reversible self-assembly of gold nanoparticles surface-immobilized with coumarin ligands. *Angew Chem Int Ed Engl* 55:936–940.
40. Ngai T, Wu C, Chen Y (2004) Effects of temperature and swelling on chain dynamics during the sol-gel transition. *Macromolecules* 37:987–993.
41. Compton OC, Osterloh FE (2007) Evolution of size and shape in the colloidal crystal-lization of gold nanoparticles. *J Am Chem Soc* 129:7793–7798.